ARTICLE

Sensitive and Label-Free Detection of Protein Secondary Structure by Amide III Spectral Signals using Surface-Enhanced Raman Spectroscopy

Kang-zhen Tian[a], Chang-chun Cao[b], Xin-ming Nie[a*], Wen Wang[a], Cai-qin Han[a*]

a. Jiangsu Key Laboratory of Advanced Laser Materials and Devices, School of Physics and Electronic Engineering, Jiangsu Normal University, Xuzhou 221116, China
b. The 95979 Army of Chinese People's Liberation Army, Taian 271200, China

(Dated: Received on November 24, 2018; Accepted on January 26, 2019)

Proteins and peptides perform a vital role in living systems, however it remains a challenge for accurate description of proteins at the molecular level. Despite that surface-enhanced Raman spectroscopy (SERS) can provide the intrinsic fingerprint information of samples with ultrahigh sensitivity, it suffers from the poor reproducibility and reliability. Herein, we demonstrate that the silver nanorod array fabricated by an oblique angle deposition method is a powerful substrate for SERS to probe the protein secondary structures without exogenous labels. With this method, the SERS signals of two typical proteins (lysozyme and cytochrome c) are successfully obtained. Additionally, by analyzing the spectral signals of the amide III of protein backbone, the influence of concentration on the folding status of proteins has been elucidated. With the concentration increasing, the components of α-helix and β-sheet structures of lysozyme increase while the secondary structures of cytochrome c almost keep constant. The SERS method in this work offers an effective optical marker to characterize the structures of proteins.

Key words: Surface-enhanced Raman spectroscopy, Silver nanorod, Protein secondary structures

I. INTRODUCTION

Proteins play a decisive role in regulating many biological activities and functions, including ion transport, signal regulation, immune response, membrane assembly, and so on [1–4]. The specific folding state of proteins determines their properties and functions, while the misfolding of the proteins can lead to various diseases, such as Parkinson, Alzheimer's disease, diabetes mellitus, and mad cow disease [5, 6]. Therefore, a comprehensive understanding of the protein folding is the key to elucidating the mechanisms of protein misfolding diseases and searching for the drug targets. Structure determination of proteins holds the key for understanding and controlling the functionality of biological systems. Many approaches are being applied to study protein folding, such as UV-Vis absorption spectroscopy [7, 8], circular dichroism (CD) [9, 10], X-ray crystallography [11, 12], IR spectroscopy [13], and Raman spectroscopy [14–16]. For example, Asher group did a lot of significant studies on the protein folding using UV-Raman [14–16].

As a highly sensitive molecular detection method, surface-enhanced Raman spectroscopy (SERS) has been proven powerful for detecting a wide variety of chemical and biological targets such as DNA [17], carbohydrates [18], and bacteria [19], at extremely low concentrations. SERS can dramatically enhance the Raman scattering signal when molecules adsorb on the surfaces of the nanostructure of the noble metal such as Au and Ag. The enhancement factor can be as big as 10^6 to 10^{11}, which means that the sensitivity even reaches the single-molecule level [20, 21]. Therefore, SERS has been widely used to study protein structure and dynamics [22–26]. For example, Xu *et al.* detected molecular vibrations in single hemoglobin (Hb) protein molecules attached to isolated or immobilized silver nanoparticles by SERS [22]. Guerrini *et al.* developed a SERS-based sensor for the detection of the oncoprotein c-Jun using silver nanoparticles (AgNPs) substrate with a peptide receptor chemically modified by covalent attachment of a thiophenol group [23]. Pazos *et al.* measured c-MYC protein using a highly sensitive SERS assay which was fabricated by coating silver nanoparticles on specifically designed hybrid materials [24]. Xu *et al.* obtained high-quality SERS signals of five typical proteins using Ag nanoparticles (AgNPs) modified by an iodide [25]. In addition, some other nano structures were also applied to investigate protein structures, such as core-shell nanoparticles [26]. In summary, the appropriate substrate is the premise and key of SERS. Thus, substantial attempts were made to fabricate the SERS-

*Authors to whom correspondence should be addressed. E-mail: nxinming@jsnu.edu.cn, hancq@jsnu.edu.cn

active metallic nanostructures for the identification of proteins.

In recent years, oblique angle deposition (OAD) has been widely utilized in plasmonic applications [27–30]. OAD method shows many advantages in controlling the size, shape, and composition of metallic nanostructures. Meanwhile, the SERS substrates fabricated by OAD method show excellent sensitivity and reproducibility [31–33]. Consequently, they have already been widely used in various fields of research, such as food safety, environmental monitoring, and biological testing. For example, Han *et al.* obtained the amount of saccharin sodium in soft drinks using the silver nanorod (AgNR) array substrates [31]. Chen *et al.* acquired the SERS spectra of seven polycyclic aromatic hydrocarbon (PAH) compounds and compared their experimental spectra with theoretical Raman spectra calculated by density function theory (DFT) [34]. Zhao *et al.* reported the direct detection of red blood cells infected by malaria based on silver nanorod array substrates [35].

In this study, we used the highly sensitive AgNR array substrates fabricated by OAD to detect the secondary structures of proteins, including lysozyme and cytochrome c. We elucidated the influence of concentration on the peptide folding status by analyzing the spectral signals of amide III of protein backbone. Herein, we provide a new potential method for rapid identification of protein secondary structures without extraneous labels.

II. EXPERIMENTS

A. Materials and sample preparations

Chicken egg white lysozyme and cytochrome c were purchased from Sangon Biotech (Shanghai) Co. Ltd. with a minimum purity of 98%. They were used without further purification. High-purity water (Milli-Q, $\geq$18.2 MΩ) was used in all experiments.

B. Fabrication of AgNR array substrates

The AgNR array substrates were fabricated by the OAD method in a custom-built e-beam deposition system (DE500, DE Technology Inc., Beijing, China). Details regarding the OAD theory and instruments have been reported in our early studies [32, 33]. We introduce them briefly here to avoid the overlap. The 1 cm$\times$1 cm square cleaned glass pieces were fixed to the deposition chamber. The deposition process was started when the pressure of the chamber reached 5×10^{-7} torr. Firstly, a 20 nm titanium film and a 100 nm silver film were deposited successively onto the glass substrates at a vapor incident angle θ=0° with respect to the surface of the substrate. Then, the substrate surface normal was rotated to an angle of 86° with respect to the vapor incident direction, and silver continued to be deposited at a rate of 0.3 nm/s. The schematic diagram of the AgNR array substrate fabricated by OAD method and the growth process are shown in FIG. 1 (a) and (b) [33].

The surface morphology of AgNR array substrate was observed by a field-emission scanning electron microscope (FESEM, SU8010, Hitachi, Tokyo, Japan). The extinction spectrum of AgNR array substrate was obtained using a UV-Vis spectrophotometer (Thermo Scientific Evolution 220) at room temperature.

C. SERS measurements

Details about SERS theories and instruments have been reported previously [34–36]. The experimental setups are similar to those described in our early studies [32, 33]. All of the SERS experiments in this research were carried out at 25 °C by a Raman analyzer (ProRaman-L-785A2, Enwave Optronics, Irvine, CA) equipped with a 785 nm diode laser. The solutions of model proteins with different concentrations were prepared in water. 2 μL of the samples were added onto the AgNR array substrate, and then dried under ambient conditions. Finally, the SERS measurement was performed with a laser power of 30 mW and an integration time of 10 s. At least 10 randomly sampled spots were measured from each sample dried on the AgNR array substrate to ensure the statistics. The SERS enhance factor (EF) was calculated using the Raman spectra of 1000 mg/L protein solution, and SERS spectra were obtained from AgNR array with 100 mW laser power and 10 s integration time.

All of the SERS spectra were plotted using Origin 8.5 (Origin Lab, Northampton, MA). The Raman shifts and SERS intensities were obtained through fitting the bands with the Lorentzian function [37].

III. RESULTS AND DISCUSSION

A. Characterization of AgNR array substrates

The top-view and cross-sectional view SEM images of the AgNR array substrate fabricated by OAD are shown in FIG. 1 (c)–(f). The result shows that AgNR array substrate distributes highly uniformly. Further measurements show that the lengths of nanorod L are (900±90) nm with a tilting angle of approximately 73° relative to the substrate normal. Across the magnified SEM images, a diameter d=(150±40) nm and a gap between adjacent rods S=(100±30) nm are defined, respectively.

The extinction spectra of the AgNR array substrates are shown in FIG. 1(g). It can be clearly observed that the UV-Vis band was located at 580 nm.

The uniformity and reproducibility of the AgNR substrates have also been evaluated. We randomly selected

DOI:10.1063/1674-0068/cjcp1811267

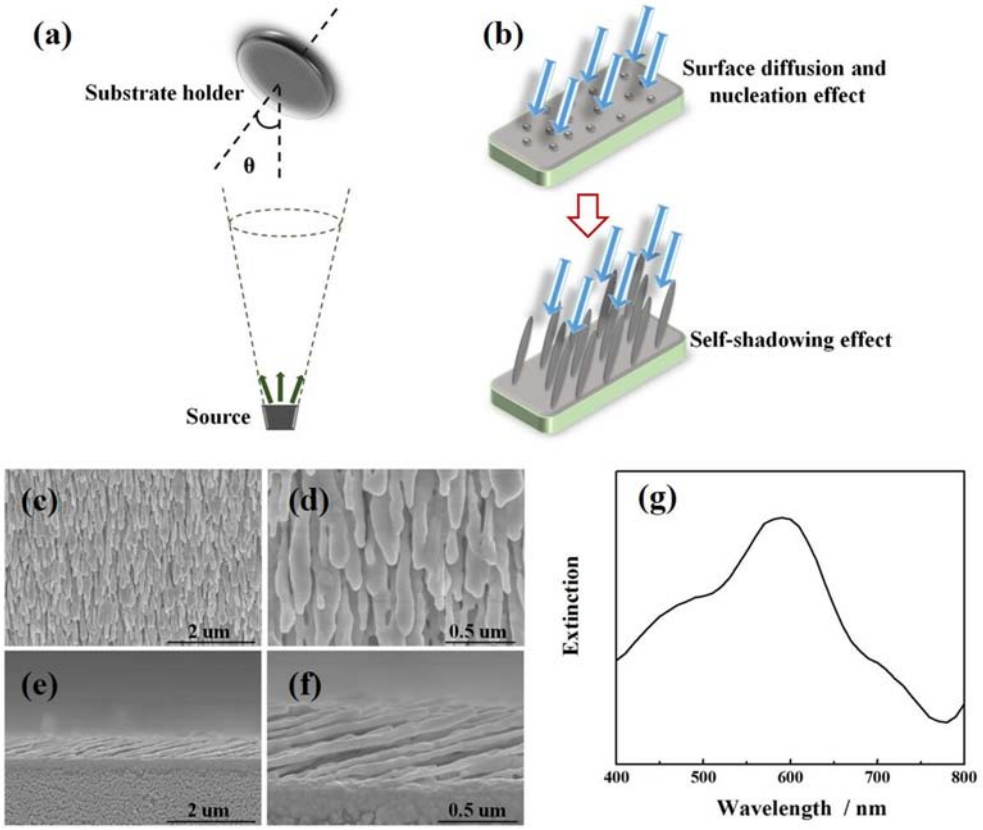

FIG. 1 (a) Schematic diagram of the AgNR array substrate fabricated by OAD method. (b) The growth process of AgNR array substrates. (c)–(f) SEM images of the AgNR array substrate. (g) Extinction spectra of AgNR array substrate.

three AgNR array substrates of the same batch. Then, we added 2 μL of 10^{-5} mol/L solution of BPE to the surfaces of these 3 substrates and collected 10 different random points from each substrate. Moreover, SERS spectra of BPE on the AgNR array substrates from 20 different batches were also collected to show the batch-to-batch reproducibility. The results are shown in FIG. 2. The relative standard deviations (RSDs) of SERS intensity for 10^{-5} mol/L BPE at $\Delta\nu$=1200 cm^{-1} are 4% and 8% for spot-to-spot and batch-to-batch measurements respectively, which indicates the high uniformity and reproducibility of the AgNR array substrates used in this study.

B. SERS performance of AgNR array substrates for the model proteins detection

In order to prove the SERS activity of AgNR array substrate, the SERS spectrum and the Raman spectrum were obtained (FIG. 3). According to previous report [32, 33], the EF of AgNR substrate was calculated by the following equations:

$$\mathrm{EF} = \left(\frac{I_{\mathrm{SERS}}}{I_{\mathrm{Raman}}}\right) \times \left(\frac{N_{\mathrm{Raman}}}{N_{\mathrm{SERS}}}\right) \tag{1}$$

$$N_{\mathrm{SERS}} = C_{\mathrm{SERS}} V_{\mathrm{SERS}} \times \frac{S_{\mathrm{Laser}}}{S_{\mathrm{SERS}}} \times \frac{N_{\mathrm{A}}}{M} \tag{2}$$

$$N_{\mathrm{Raman}} = C_{\mathrm{Raman}} V_{\mathrm{Laser}} \times \frac{N_{\mathrm{A}}}{M} \tag{3}$$

where I_{SERS} is the SERS intensity of protein solution (C_{SERS}=50 mg/L) recorded from AgNR array substrate and I_{Raman} is the bulk Raman intensity of protein solution (C_{Raman}=50 mg/L). Besides, N_{SERS} and N_{Raman} are the estimated amount of protein molecules contributed to SERS and Raman spectrum, respectively. The volume of protein solution added to the AgNR array substrate surface was V_{SERS}=2 μL and the solution was spread in circularity with the diameter of 2 mm, so $S_{\mathrm{SERS}}=3.14\times10^{-6}$ m^2. $S_{\mathrm{Laser}}=\pi r^2=7.6\times10^{-12}$ m^2 ($r=1.56\times10^{-6}$ m) is the calculated laser beam area at the substrate surface. The volume of protein solution produced Raman scattering was calculated to be $V_{\mathrm{Laser}}=2.5\times10^{-12}$ m^3. N_{A} is the Avogadro constant ($N_{\mathrm{A}}=6.02\times10^{23}$ mol^{-1}), and M is the molar mass of proteins. The EF of AgNR substrate in this study was finally calculated by the following equation:

$$\mathrm{EF} = \left(\frac{I_{\mathrm{SERS}}}{I_{\mathrm{Raman}}}\right) \times \left(\frac{V_{\mathrm{Laser}}}{V_{\mathrm{SERS}}}\right) \times \left(\frac{S_{\mathrm{SERS}}}{S_{\mathrm{Laser}}}\right) \tag{4}$$

Based on peak intensities of lysozyme at 760 cm^{-1},

DOI:10.1063/1674-0068/cjcp1811267

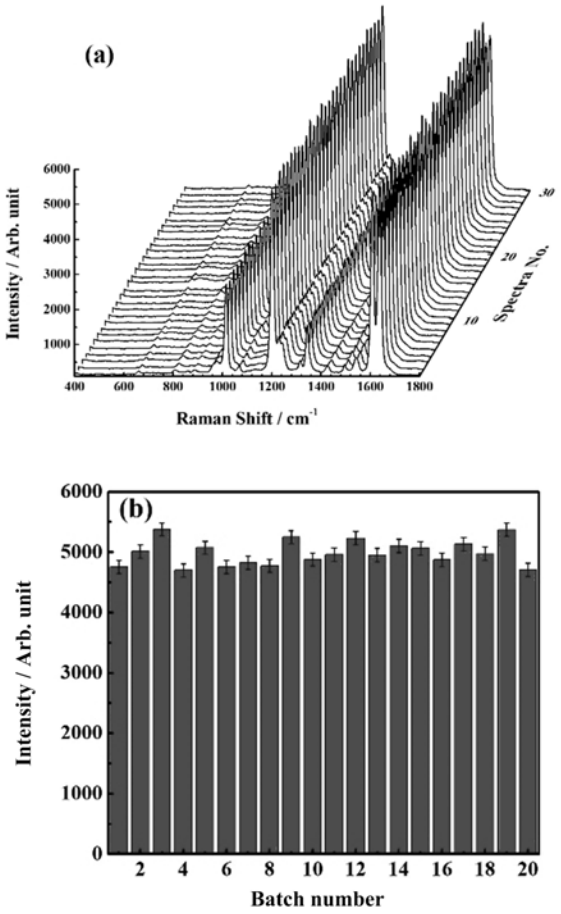

FIG. 2 (a) SERS spectra of 30 randomly selected spots from 3 different substrates of the same batch. (b) $I_{1200\ \mathrm{cm^{-1}}}$ from 20 different batches of AgNR samples. Error bars show the standard deviations.

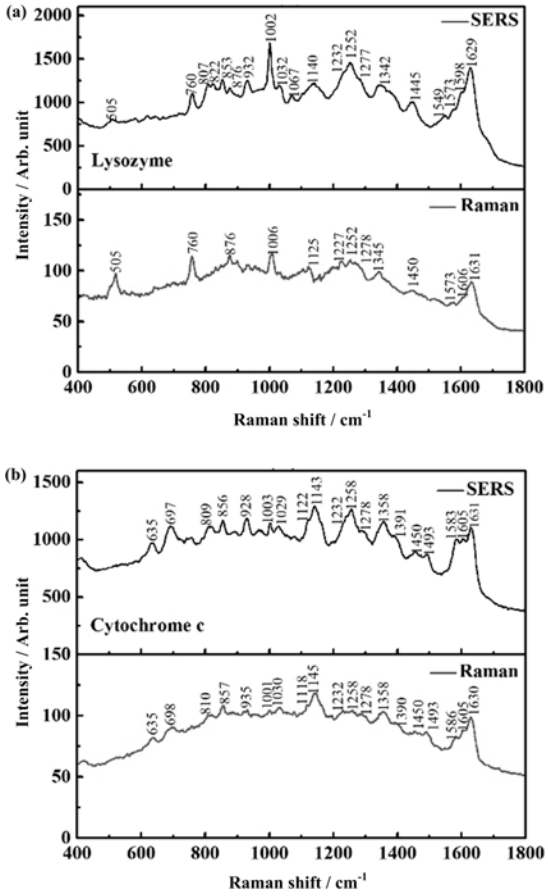

FIG. 3 SERS and Raman spectra of (a) lysozyme and (b) cytochrome c.

the EF of AgNR array substrate for lysozyme was calculated to be $\sim 5\times10^3$. Similarly, the EF of AgNR array substrate for cytochrome c was calculated to be $\sim 5.8\times10^3$ based on peak intensities of lysozyme at 1358 $\mathrm{cm^{-1}}$. In addition, considering the higher concentration of solution and laser energy used in Raman experiment than SERS experiment, the enhancement factor should be larger. The results indicate that the AgNR array substrates exhibit good enhancement ability and have great promise for practical application.

From FIG. 3, we can observe that SERS spectra of lysozyme and cytochrome c show abundant vibrational peaks with good signal-to-noise ratio, such as the stretching vibration of disulfide (SS) bridges (505 $\mathrm{cm^{-1}}$). The vibrations of the side chains of the amino acids can also be observed clearly from FIG. 3, such as Tyr (807, 822, 853 $\mathrm{cm^{-1}}$), Phe (1002, 1032 $\mathrm{cm^{-1}}$), and Trp (760, 1342, 1549 $\mathrm{cm^{-1}}$) of lysozyme [25, 38–40]. Similarly, the typical vibrational peaks of cytochrome c can also be observed, including Tyr (809, 856 $\mathrm{cm^{-1}}$), Phe (1003, 1029 $\mathrm{cm^{-1}}$), and Trp (1358 $\mathrm{cm^{-1}}$) [40–42]. Meanwhile, amide backbones vibrational modes of the proteins above were also detected, which provided important information of the constituent and structure of proteins [25, 37, 41, 42]. The bands in the 1600–1700 $\mathrm{cm^{-1}}$ region are regarded as amide I modes, which consists mainly of C=O stretching and a small amount of out-of-phase C−N stretching. The amide I vibration has been used for secondary structure analysis in previous studies because it depends on the secondary structure of the backbone [43, 44]. However, the drawback is that the characteristic amide I bands of various secondary structures are clustered in the spectral region of 1600–1700 $\mathrm{cm^{-1}}$, resulting in the difficulty of attribution. For example, it is difficult to distinguish α-helix and random-coil structures because of the overlap of their frequencies at $\sim$1655 $\mathrm{cm^{-1}}$ [41–45]. Consequently, it becomes extremely difficult to acquire accurate structural information of proteins if we only analyze the spectral region of the vibrations of amide I.

The difficulties of attribution associated with amide I bands could be effectively resolved when amide III bands are considered. The amide III vibrations (between 1200 and 1400 $\mathrm{cm^{-1}}$) come from the in-phase combinations of C−N stretching and N−H bending

DOI:10.1063/1674-0068/cjcp1811267

TABLE I Assignment of vibrational bands (in cm^{-1}) for lysozyme and cytochrome c in Raman and SERS spectra.

Assignment	Bands of lysozyme		Bands of cytochrome c	
	Raman	SERS	Raman	SERS
ν(SS)	505	505		
Tyr			635	635
ν(CS)			698	697
Trp-indole breathing (W18)	760	760		
Tyr/ν(C−S−C)		807	810	809
Tyr Fermi doublet		822		
Tyr Fermi doublet		853	857	856
Tyr	876	876		
Main chain vibration $\nu(C_\alpha-C)$		932	935	928
Phe-ring breathing	1006	1002	1001	1003
Phe		1032	1030	1029
ν(CN)		1067	1118	1122
ν(CN)	1125	1140	1145	1143
Amide III (β-sheet)	1227	1232	1232	1232
Amide III (random-coil)	1252	1252	1258	1258
Amide III (α-helix)	1278	1277	1278	1278
Trp-indole ring (C−H deformation)	1345	1342		
Trp				1358
COO^- symmetric stretching			1390	1391
$\delta(CH_2)$	1450	1445	1450	1450
His			1493	1493
Trp-indole ring stretching		1549		
Trp-W2 mode	1573	1573		
$\nu(C_\alpha-C_m)$asym			1586	1583
Phe/Tyr	1606	1598		
$\nu(C_\beta-C_\beta)$			1605	1605
Tyr	1631	1629	1630	1631

[4, 41]. They are highly sensitive to the peptide bond conformation and thus can probe the protein secondary structures. In general, compared with amide I, the amide III signals are much weaker, resulting in the measurement being more difficult. Recently, the studies using sum frequency generation vibrational spectroscopy have verified that the amide III signals are capable of directly distinguishing α-helix, random-coil, β-sheet, and turn-like structures in proteins [2, 43, 46–49]. In this study, we enhance the signals in the fingerprint region successfully by AgNR array substrates. As shown in FIG. 3, the characterized spectral features of α-helix, random-coil, and β-sheet are found in the positions of $\sim$1277 cm^{-1}, $\sim$(1255±3) cm^{-1}, and $\sim$1232 cm^{-1}, respectively [40–42]. The detailed band assignments for the SERS spectra of lysozyme and cytochrome c are presented in Table I.

It is observed that the amide III signals are largely enhanced on the AgNR array substrate while the amide I signals are suppressed, which may be due to the orientation. For example, in the α-helix structure, the transition dipole of the amide I lies along the α-helix direction, while the amide III vibrates perpendicularly to it. In this study, the protein lies on the surface. Therefore, the transition dipole of the amide I lies on the surface and is perpendicular to the electric field of surface plasmon. In contrast, the transition dipole of the amide III is perpendicular to the surface and lies along the electric field of surface plasmon. As a result, the amide III signals are largely enhanced and the amide I signals are suppressed

C. The influence of concentration on secondary structures of lysozyme

After obtaining the experimental method as described above, we started to investigate the transition of secondary structures of model proteins at different concentrations. FIG. 4 shows the SERS spectra of lysozyme at different concentrations. We can observe that the vibration signals of protein secondary structure become obvious with the increase of concentration. In order to further explore the influence of concentration on the

DOI:10.1063/1674-0068/cjcp1811267

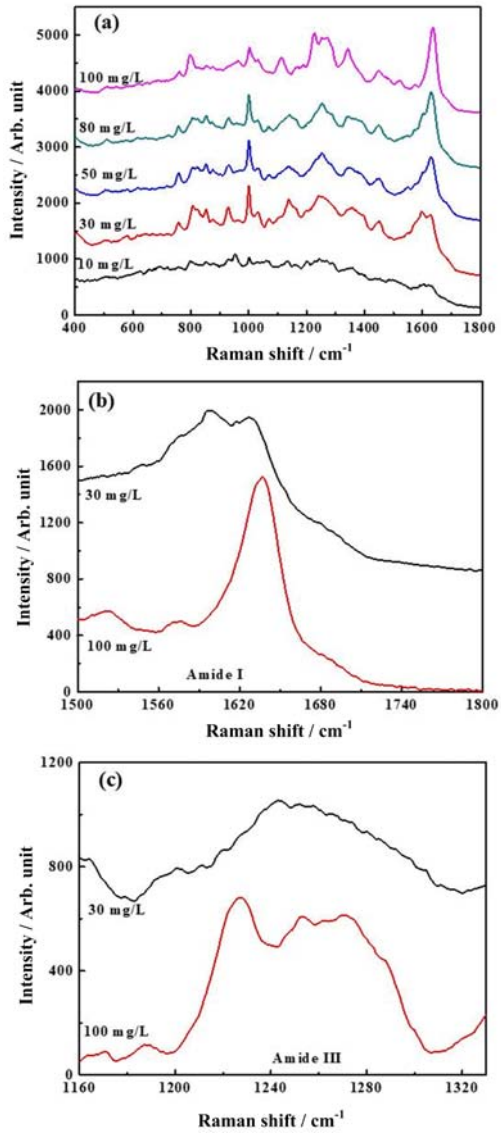

FIG. 4 Surface-enhanced Raman spectra of lysozyme at different concentrations: (a) full spectra, (b) amide I spectra region, and (c) amide III spectra region (30 mg/L for black line and 100 mg/L for red line).

folding structures, the SERS spectra of amide I region and amide III region of the lysozyme are plotted in FIG. 4 (b) and (c). From FIG. 4(b), we can observe that there is a strong peak at ∼1629 cm^{-1}. Previous studies indicate that the ∼1629 cm^{-1} peak contributes to the Tyr structure [37–42]. It becomes difficult to accurately distinguish α-helical and random-coil structures because of the overlap of their frequencies. FIG. 4(c) shows amide III signals of lysozyme and we can observe that the amide III spectra are dominated by three peaks centering at ∼1232, ∼1252, and ∼1277 cm^{-1}. According to Raman spectral features, these peaks are assigned to β-sheet, random-coil, and α-helix respectively [4, 40, 43]. The amide III spectra indicate that lysozyme adopts both α-helix and random-coil structures. This conclusion is difficult to obtain from the spectrum of amide I.

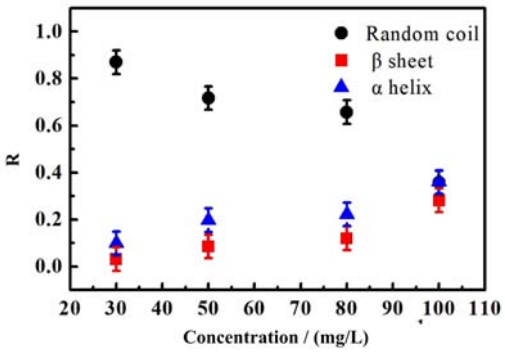

FIG. 5 Percentages of different secondary structures of lysozyme at different concentrations, obtained by the analysis of the amide III region.

In order to further quantitatively analyze the secondary structures of protein, we fitted the SERS spectra in FIG. 4. Previous studies indicate that the strength ratios for the peaks can be employed to determine the protein secondary structures [2, 50, 51]. Percentages of different secondary structures of lysozyme obtained by the analysis of the amide III Raman region at different concentrations are shown in FIG. 5. It is found that the structure of the lysozyme at low concentrations is mainly the random-coil type with tiny α-helix and β-sheet types. With the concentration increasing, the ratio of random-coil structure decreases and reaches about 36% when the concentration is 100 mg/L. In contrast, the ratios of α-helix and β-sheet structure increase to 36% and 28%, respectively. The results indicate that high concentration of lysozyme promotes the transformation of structure from the random-coil type into α-helix and β-sheet types. It is obvious that this SERS spectral approach can enhance our ability to monitor the secondary structures of proteins.

D. The influence of concentration on the secondary structures of cytochrome c

In order to further prove the effectiveness and universality of the SERS method as described above, we have also investigated the influence of concentration on the secondary structures of cytochrome c. FIG. 6 shows the SERS spectra of cytochrome c at different concentrations and FIG. 6(b) shows the amide I SERS spectra region of cytochrome c for a better comparison. As shown in FIG. 6(b), the spectra are dominated by several peaks at ∼1583, ∼1605, and ∼1631 cm^{-1}. The peaks at ∼1583 and ∼1605 cm^{-1} are assigned to the $C_\alpha-C_m$ and $C_\beta-C_\beta$ stretches, respectively [40–42, 52]. The ∼1631 cm^{-1} peak is mainly attributed to the Tyr structure. The study of lysozyme above has demonstrated that the amide III spectral signal can differenti-

DOI:10.1063/1674-0068/cjcp1811267

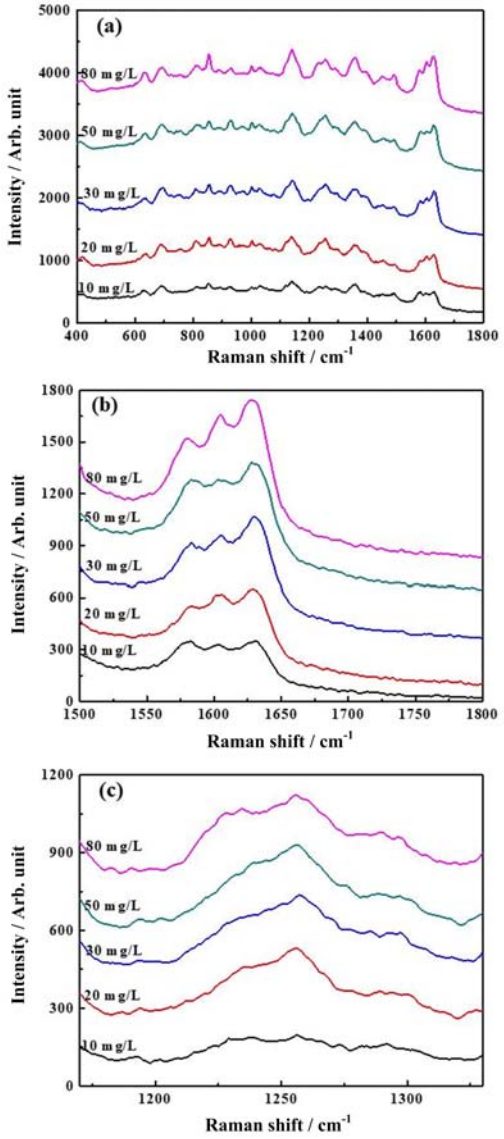

FIG. 6 Surface-enhanced Raman spectra of cytochrome c with different concentrations: (a) full spectra, (b) amide I spectra region, and (c) amide III spectra region.

ate the protein secondary structures effectively. It can be seen from FIG. 6(c) that the amide III spectra of the cytochrome c are dominated by three peaks at ∼1232, ∼1258, and ∼1278 cm^{-1}, which are originated from β-sheet, random-coil, and α-helix structure, respectively [40–42].

In order to qualitatively analyze the secondary structures of cytochrome c, we fitted the amide III spectra in FIG. 6(c). We also calculated the components of different secondary structures and the results are shown in FIG. 7. It can be observed that cytochrome c predominantly adopts a random-coil structure (∼62%) with tiny α-helix (∼17%) and β-sheet (∼21%) structures. Furthermore, the composition of protein secondary structure is stable at different concentrations.

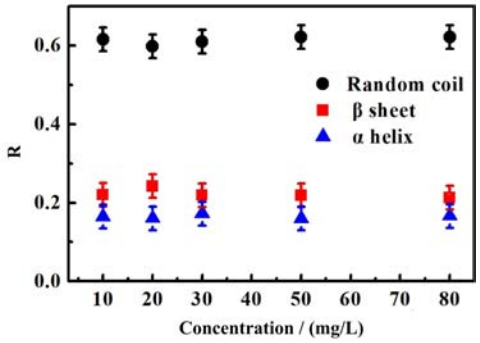

FIG. 7 Percentages of different secondary structures of cytochrome c at different concentrations, obtained by the analysis of the amide III region.

Overall, our results show the advantages of using SERS based on silver nanorod array to probe protein structures. Meanwhile, the effectiveness of analyzing amide III signals to differentiate the protein secondary structures is demonstrated in this study. Because we cannot directly get molecular mechanism information only by SERS, such as protein binding affinity, surface abundance, and adsorption homogeneity. The molecular mechanism of protein folding needs further studies.

IV. CONCLUSION

In this study, the AgNR array substrate fabricated by OAD has been successfully applied for obtaining SERS signals of two model proteins (lysozyme and cytochrome c). This study demonstrates that the effectiveness of analyzing amide III signals differentiates the protein secondary structures. The well-separated spectral peaks of the protein secondary structure in the amide III region provide direct structural information of proteins. The spectral results also indicate that high concentration promotes the transformation of lysozyme from random-coil to α-helix and β-sheet structures, while secondary structures of cytochrome c remain stable at different concentrations. Using this SERS method, we can monitor the secondary structures of proteins better.

V. ACKNOWLEDGMENTS

This work was supported by the National Natural Science Foundation of China (No.61805109 and No.61575087), the Natural Science Foundation of Jiangsu Province (No.BK20170229), the Natural Science Foundation of the Higher Education Institutions of Jiangsu Province (No.18KJB180004 and No.16KJB510009), and the Natural Science Foundation of Jiangsu Normal University (No.16XLR021)

DOI:10.1063/1674-0068/cjcp1811267

[1] Z. Wang, S. Zong, L. Wu, D. Zhu, and Y. Cui, Chem. Rev. **117**, 7910 (2017).
[2] S. Ye, H. Li, W. Yang, and Y. Luo, J. Am. Chem. Soc. **136**, 1206 (2014).
[3] H. Kitoh-Nishioka, D. Yokogawa, and S. Irle, J. Phys. Chem. C **121**, 4220 (2017).
[4] S. A. Oladepo, K. Xiong, Z. Hong, S. A. Asher, J. Handen, and I. K. Lednev, Chem. Rev. **112**, 2604 (2012).
[5] M. Wang and R. J. Kaufman, Nature **529**, 326 (2016).
[6] K. Rajasekhar, N. Narayanaswamy, N. A. Murugan, K. Viccaro, H. G. Lee, K. Shah, and T. Govindaraju, Biosens. Bioelectron. **98**, 54 (2017).
[7] Y. Song, R. E. Haddad, S. L. Jia, S. Hok, M. M. Olmstead, D. J. Nurco, N. E. Schore, J. Zhang, J. G. Ma, K. M. Smith, S. Gazeau, J. Pécaut, J. C. Marchon, C. J. Medforth, and J. A. Shelnutt, J. Am. Chem. Soc. **127**, 1179 (2005).
[8] J. M. Antosiewicz and D. Shugar, Biophys. Rev. **8**, 163 (2016).
[9] J. L. Lopes, A. J. Miles, L. Whitmore, and B. A. Wallace, Protein Sci. **23**, 1765 (2014).
[10] L. Whitmore, L. Mavridis, B. A. Wallace, and R. W. Janes, Protein Sci. **27**, 10 (2018).
[11] Y. O. Jung, J. H. Lee, J. Kim, M. Schmidt, K. Moffat, V. Šrajer, and H. Ihee, Nat. Chem. **5**, 212 (2013).
[12] K. B. Handing, E. Niedzialkowska, I. G. Shabalin, M. L. Kuhn, H. Zheng, and W. Minor, Nat. Protoc. **13**, 1062 (2018).
[13] F. Zeeshan, M. Tabbassum, L. Jorgensen, and N. J. Medlicott, Appl. Spectrosc. **72**, 268 (2018).
[14] Z. Hong, J. Wert, and S. A. Asher, J. Phys. Chem. B **117**, 7145 (2013).
[15] D. Punihaole, R. S. Jakubek, R. J. Workman, and S. A. Asher, J. Phys. Chem. Lett. **9**, 1944 (2018)
[16] S. A. Oladepo, K. Xiong, Z. Hong, S. A. Asher, J. Handen, and I. K. Lednev, Chem. Rev. **112**, 2604 (2012).
[17] L. J. Xu, Z. C. Lei, J. Li, C. Zong, C. J. Yang, and B. Ren, J. Am. Chem. Soc. **137**, 5149 (2015).
[18] D. Sun, G. Qi, F. Cao, W. Xu, Q. Chen, and S. Xu, Talanta **171**, 159 (2017).
[19] H. Zhou, D. Yang, N. P. Ivleva, N. E. Mircescu, R. Niessner, and C. Haisch, Anal. Chem. **86**, 1525 (2014).
[20] P. L. Stiles, J. A. Dieringer, N. C. Shah, and R. P. Van Duyne, Ann. Rev. Anal. Chem. **1**, 601 (2008).
[21] F. H. Cho, Y. C. Lin, and Y. H. Lai, Appl. Surf. Sci. **402**, 147 (2017).
[22] H. Xu, E. J. Bjerneld, M. Käll, and L. Börjesson, Phys. Rev. Lett. **83**, 4357 (1999).
[23] L. Guerrini, E. Pazos, C. Penas, M. E. Vázquez, J. L. Mascareñas, and R. A. Alvarez-Puebla, J. Am. Chem. Soc. **135**, 10314 (2013).
[24] E. Pazos, M. Garcia-Algar, C. Penas, M. Nazarenus, A. Torruella, N. Pazos-Perez, L. Guerrini, M. E. Vzquez, E. Garcia-Rico, J. L. Mascareñas, and R. A. Alvarez-Puebla, J. Am. Chem. Soc. **138**, 14206 (2016).
[25] L. J. Xu, C. Zong, X. S. Zheng, P. Hu, J. M. Feng, and B. Ren, Anal. Chem. **86**, 2238 (2014).
[26] S. Y. Ding, R. Panneerselvam, and Z. Q. Tian, Chem. Rev. **117**, 5002 (2017).
[27] Y. Yang, Z. Hu, Y. Wang, B. Wang, Q. Zhan, Y. Zhang, and X. Ao, Opt. Mater. Express **6**, 2644 (2016).
[28] C. Song, J. Chen, J. L. Abell, Y. Cui, and Y. Zhao, Langmuir **28**, 1488 (2012).
[29] Q. Zhou, Y. He, J. Abell, Z. Zhang, and Y. Zhao, Chem. Commun. **47**, 4466 (2011).
[30] Q. Zhou, X. Zhang, Y. Huang, Z. Li, Y. Zhao, and Z. Zhang, Appl. Phys. Lett. **100**, 113101 (2012).
[31] C. Han, Y. Yao, W. Wang, L. Qu, L. Bradley, S. Sun, and Y. Zhao, Sens. Actuators B **251**, 272 (2017).
[32] Y. Yao, W. Wang, K. Tian, W. M. Ingram, J. Cheng, L. Qu, H. Li, and C. Han, Spectrochim. Acta Part A **195**, 165 (2018).
[33] K. Tian, W. Wang, Y. Yao, X. Nie, A. Lu, Y. Wu, and C. Han, J. Raman Spectrosc. **49**, 472 (2018).
[34] J. Chen, Y. W. Huang, and Y. Zhao, J. Raman Spectrosc. **46**, 64 (2015).
[35] F. Chen, B. R. Flaherty, C. E. Cohen, D. S. Peterson, and Y. Zhao, Nanomedicine **12**, 1445 (2016).
[36] N. Feliu, M. Hassan, E. Garcia Rico, D. Cui, W. Parak, and R. Alvarez-Puebla, Langmuir **33**, 9711 (2017).
[37] L. Xing, K. Lin, X. Zhou, S. Liu, and Y. Luo, J. Phys. Chem. B **120**, 10660 (2016).
[38] G. Chandra, K. S. Ghosh, S. Dasgupta, and A. Roy, Int. J. Biol. Macromol. **47**, 361 (2010).
[39] E. Podstawka, Y. Ozaki, and L. M. Proniewicz, Appl. Spectrosc. **58**, 1147 (2004).
[40] X. Yang, C. Gu, F. Qian, Y. Li, and J. Z. Zhang, Anal. Chem. **83**, 5888 (2011).
[41] B. S. Yeo, S. Mädler, T. Schmid, W. Zhang, and R. Zenobi, J. Phys. Chem. C **112**, 4867 (2008).
[42] J. L. Lyon, R. T. Hill, J. B. Shear, and K. J. Stevenson, Anal. Chem. **79**, 2303 (2007).
[43] J. H. Huang, K. Z. Tian, S. J. Ye, and Y. Luo, J. Phys. Chem. C **120**, 15322 (2016).
[44] C. Ota and K. Takano, Langmuir **32**, 7372 (2016).
[45] B. Zhang, J. Tan, C. Li, J. Zhang, and S. Ye, Langmuir **34**, 7554 (2018).
[46] Y. Liu, J. J. Tan, J. H. Zhang, C. Z. Li, Y. Luo, and S. J. Ye, Chem. Commun. **54**, 5903 (2018).
[47] K. Meister, A. Paananen, B. Speet, M. Lienemann, and H. J. Bakker, J. Phys. Chem. B **121**, 9398 (2017).
[48] X. Hu, J. J. Tan, and S. J. Ye, J. Phys. Chem. C **121**, 15181 (2017).
[49] J. J. Tan, J. H. Zhang, Y. Luo, and S. J. Ye, J. Am. Chem. Soc. (2019), DOI: 10.1021/jacs.8b08537.
[50] A. Torreggiani, M. Tamba, I. Manco, M. R. Faraone-Mennella, C. Ferreri, and C. Chatgilialoglu, J. Mol. Struct. **744**, 767 (2005).
[51] Z. D. Schultz and I. W. Levin, Annu. Rev. Anal. Chem. **4**, 343 (2011).
[52] Q. Yu and G. Golden, Langmuir **23**, 8659 (2007).

DOI:10.1063/1674-0068/cjcp1811267